

Signature of Many-Body Localization of Phonons in Strongly Disordered Superlattices

Thanh Nguyen,¹ Nina Andrejevic,² Hoi Chun Po,³ Yoichiro Tsurimaki,⁴ Nathan C. Drucker,⁵ Ahmet Alatas,⁶ Ercan E. Alp,⁶ Bogdan M. Leu,^{6,7} Alessandro Cunsolo,⁸ Yong Q. Cai,⁸ Lijun Wu,⁹ Joseph A. Garlow,⁹ Yimei Zhu,⁹ Hong Lu,¹⁰ Arthur C. Gossard,¹¹ Shengxi Huang,^{12,*} and Mingda Li^{1,*}

¹*Department of Nuclear Science and Engineering, MIT, Cambridge, MA, 02139, USA*

²*Department of Material Science and Engineering, MIT, Cambridge, MA, 02139, USA*

³*Department of Physics, MIT, Cambridge, MA, 02139, USA*

⁴*Department of Mechanical Engineering, MIT, Cambridge, MA, 02139, USA*

⁵*John A. Paulson School of Engineering and Applied Sciences, Harvard University, Cambridge, MA 02138, USA*

⁶*Advanced Photon Source, Argonne National Laboratory, Lemont, IL, 60439, USA*

⁷*Department of Physics, Miami University, Oxford, Ohio, 45056, USA*

⁸*National Synchrotron Light Source II, Brookhaven National Laboratory, Upton, NY, 11973, USA*

⁹*Condensed Matter Physics and Material Science Department, Brookhaven National Laboratory, Upton, NY, 11973, USA*

¹⁰*College of Engineering and Applied Sciences, Nanjing University, Nanjing, China*

¹¹*Materials Department, University of California, Santa Barbara, Santa Barbara, CA, 93106, USA*

¹²*Department of Electrical Engineering, The Pennsylvania State University, University Park, PA, 16802, USA*

(Dated: April 1, 2025)

Many-body localization (MBL) has attracted significant research attention due to its immunity to thermalization, role in logarithmic entanglement entropy growth, and opportunities to reach exotic quantum orders. However, experimental realization of MBL in solid-state systems has remained challenging. Here we report evidence of a possible phonon MBL phase in disordered GaAs/AlAs superlattices. Through grazing-incidence inelastic X-ray scattering, we observe a strong deviation of the phonon population from equilibrium in disordered samples doped with ErAs nanodots at low temperature, signaling a departure from thermalization. This behavior occurs within finite phonon energy and wavevector windows, suggesting a localization-thermalization crossover. We support our observation by proposing a theoretical model for the effective phonon Hamiltonian in disordered superlattices, and showing that it can be mapped exactly to a disordered 1D Bose-Hubbard model with a known MBL phase. The large on-site repulsion qualitatively explains the experimental findings. Our work provides mode-resolved experimental evidence of phonon localization, potentially extending the scope of MBL to disordered solid-state systems.

Many-body localized (MBL) states subject to strong disorder and strong interactions provide a platform for highly unusual phenomenology [1–5]. Notable examples include the absence of thermalization upon evolution under intrinsic dynamics for parametrically long time scales, quantum phase transitions at nonzero temperatures, and novel dynamical phases of matter. In particular, MBL can protect exotic quantum orders through localization of excitations that would otherwise result in trivialization of the phases [6–8]. Hence, these systems have recently seen heightened interest by serving as a possible pathway towards quantum information processing in systems driven far from equilibrium. MBL has been the subject of exciting studies in well-controlled artificial quantum systems such as ultracold atoms [9–13], trapped ions [14], interacting spin chains [15], and superconducting circuits [16, 17]. In contrast to such isolated systems, the unavoidable environmental couplings in a solid-state system smear the sharp features of MBL [18] and thus often preclude further experimental explorations.

In parallel with MBL, the importance of phonon localization can hardly be overlooked. It is well known that interference between multiple wave scattering paths in systems with even arbitrarily weak disorder can result in Anderson localization depending on the system dimen-

sionality [19–21]. As a fundamental wave phenomenon, Anderson localization has been theoretically studied in a wide variety of systems [22–27], including phonons [28–30]. However, unlike photons [31–35] and classical waves [36] where coherence can be readily maintained, direct measurements of phonon localization had eluded experiments until recently. The observation of coherent phonons in semiconducting superlattice (SL) systems enabled the exploration of phonon-related phenomena that relied on such coherence [37]. Numerical calculations [38–40] alongside experimental evidence in heat conduction [41] established localization as a fundamental mode of phonon transport.

Nevertheless, open questions remain. Theoretical predictions suggest that phonon localization would transpire within a finite energy interval characterized by multiple mobility edges separating propagating from localized states [29, 38], but mode-resolved phonon localization is yet to be demonstrated. The strong interactions and strong disorders in phononic SL systems further calls for an MBL description of phonon localization. The elucidation of phonon localization through the lens of MBL would have major implications for connecting the MBL phenomenology to a mesoscopic solid-state system and can shed light on further avenues towards thermoelectric

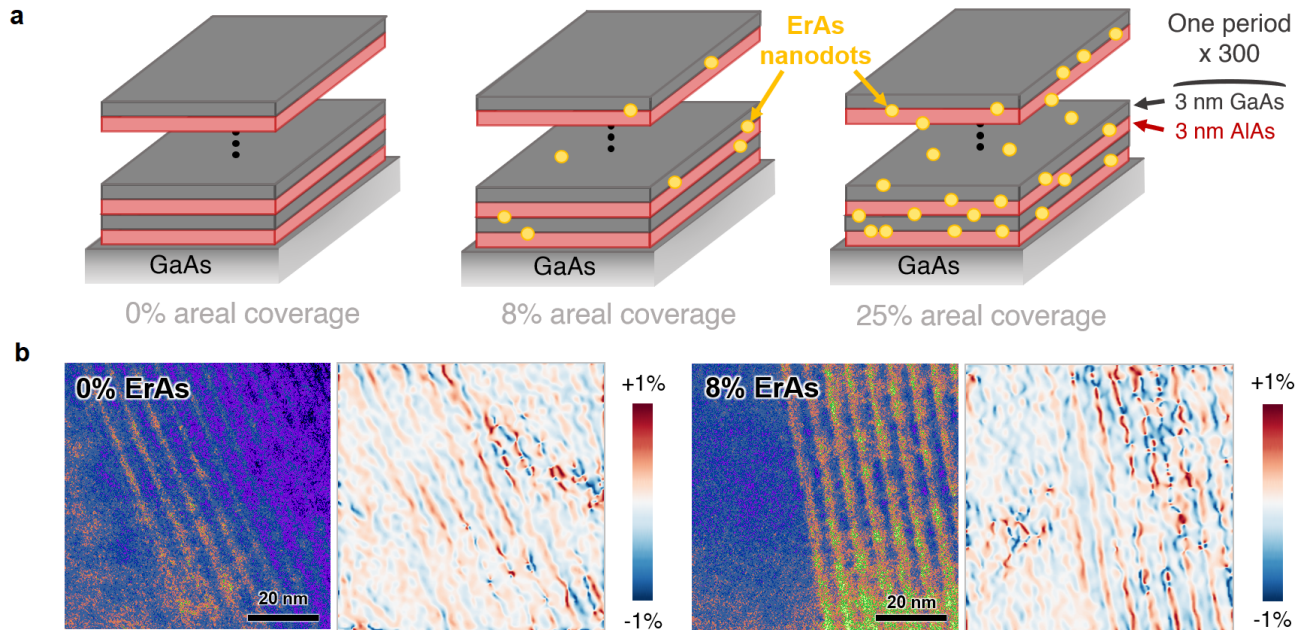


Figure 1. **GaAs/AlAs SL samples.** **a**, Illustration of the pristine Ref (0%) and disordered GaAs/AlAs SL samples with 3 nm-diameter ErAs nanodots (8% and 25% areal coverage). The SLs consist of 300 periods of 3 nm-thick GaAs and 3 nm-thick AlAs layers grown on a GaAs substrate. **b**, Transmission electron micrograph and related strain mapping of the Ref (left two images) and 8% ErAs disordered SLs (right two images).

energy conversion and thermal management in microelectronics [42].

In this work, we experimentally demonstrate a strong departure from phonon thermalization in disordered GaAs/AlAs SLs embedded with ErAs nanodots using grazing-incidence inelastic x-ray scattering (GI-IXS), which reveals a possible manifestation of MBL. Such measurements are technically challenging as they require resolving energy shifts on the order of meV with ~ 10 keV x-rays scattered off a μm -thick thin film [43]. Comparison of the phonon Stokes and anti-Stokes signals reveals persistent non-equilibrium conditions of the phonon population when disordered ErAs nanodots are introduced. This is suggestive of an MBL phase which is characterized by an effective temperature that deviates from its thermal value in a canonical ensemble [44–46]. This anomalous behavior occurs systematically within a range of phonon energies and wavevectors at low temperature, revealing a crossover behavior of MBL. We support our experimental results through an exact theoretical mapping between an effective phonon Hamiltonian for disordered SLs and the 1D Bose-Hubbard model with a known MBL phase. Our work presents strongly disordered SL systems as a promising setting to further explore MBL phenomena in solid-state systems.

Sample characterization. The samples in the GI-IXS experiments comprise three sets of 300-period

GaAs/AlAs SLs epitaxially grown on a GaAs (001) substrate. They possess a superperiodicity of 6 nm consisting of a 3 nm GaAs layer followed by a 3 nm AlAs layer. Two disordered SLs are embedded with randomly-distributed 3 nm-diameter ErAs nanodots: one with an areal density of 8% and the other, 25% (Fig. 1a). The average ErAs interparticle distance is 9.5 nm and 5.5 nm, respectively. The third, pristine SL with 0% nanodot density is kept as a reference (hereafter referred to as "Ref"). All samples were grown by molecular beam epitaxy (MBE) in a Veeco Gen III MBE system. The sub-monolayer ErAs deposition was inserted at the SL interfaces, and the formation of nanodots are caused by the self-assembly of deposited atoms. The size of the ErAs nanodots and the inter-nanodot distances are comparable to the SL superperiodicity, indicating a strong effect of ErAs disorder, in contrast to point-like impurities. Transmission electron microscope-based strain mapping (Fig. 1b) shows a low and uniform strain distribution across the SLs, indicating high-quality growth of disordered-SL at similar strain level of Ref-SL. Further characterizations of these samples can be found in [41].

Non-specular GI-IXS experiments were carried out at beamline 3-ID-C in Advanced Photon Source at Argonne National Lab [47–50]. A schematic is illustrated in Fig. 2a. With an incident x-ray energy of $E_i = 21.7$ keV, a grazing incident angle of $\theta_i = 0.5^\circ$ was chosen such that the corresponding probing depths $\lambda_a(\text{GaAs}) = 0.46 \mu\text{m}$

and $\lambda_a(\text{AlAs}) = 0.82 \mu\text{m}$ are comparable to the $1.8 \mu\text{m}$ total SL thickness. This indicates a dominant scattering contribution from the SL rather than from the substrate. Given the large E_i (corresponding to a wavevector $k_i = 110 \text{ nm}^{-1}$) and small θ_i , the x-ray wavevector transfer $q \equiv k_i - k_f$ is largely in the out-of-plane direction of the SL in the measured range up to 29.9 nm^{-1} , indicating quasi-1D phonon measurements. Constant- q scans of the energy transfer ($E \equiv E_i - E_f$) were performed for all samples at eight different q values, of which three representative ones at low, medium and high values are shown in Fig. 2b (other values in Figs. S1-S2). These measurements were performed at an optimized low temperature of 30 K to balance between the long phonon coherence length and the high phonon population [38], and at room temperature.

At low- q values ($q = 10.5 \text{ nm}^{-1}$ in Fig. 2b), the spectra of the Ref SL and disordered SLs behave similarly by nearly overlapping each other. The low phonon and high elastic peak intensities make it difficult to quantitatively extract the phonon dispersion in this SL system. As one accesses to medium- q values ($q = 23.3 \text{ nm}^{-1}$ in Fig. 2b), the behavior of the anti-Stokes ($E < 0$) and Stokes ($E > 0$) peaks become highly unusual. Thermodynamic equilibrium dictates that the Stokes/anti-Stokes amplitude ratio satisfies detailed balance where at high temperatures, this ratio approaches unity, and at low temperatures, the Stokes peak intensity dominates over that of the anti-Stokes signal. All samples, irrespective of ErAs content, follow this tendency at low- q and high- q regimes for both temperatures. However, two key discrepancies are discernible in the medium- q range. First, whereas the Ref SL sample shows significantly larger Stokes peak intensity at low temperature, the disordered SL samples have surprisingly comparable intensities for both anti-Stokes and Stokes peaks at low temperature, highlighting a departure from thermal equilibrium. An attribution to the exciton resonance effect [51] is easily excluded due to the distinct energy scale and temperature profile, and all measured SLs are electrically insulating with no exciton effects. Second, the presence of disorder drastically decreases phonon intensities relative to the elastic peak, indicating a suppressed phonon population [52]. This behavior is most prominent at $q = 23.3 \text{ nm}^{-1}$ but can also be found in nearby q values. This would point towards delimiting a finite regime of wavevectors where the phonons do not properly thermalize. Moreover, the phonon spectra at $q = 23.3 \text{ nm}^{-1}$ and low-temperature has a broad linewidth indicates a high relaxation rate, which further suggests a strong phonon interaction that may facilitate the MBL formation. At high- q values ($q = 29.9 \text{ nm}^{-1}$ in Fig. 2b), the spectra between the Ref SL and disordered SLs largely overlap again. A small energy shift between the Ref SL and disordered SLs is observed, which may be attributed to the effect of disorder on the phonon energy. All of these

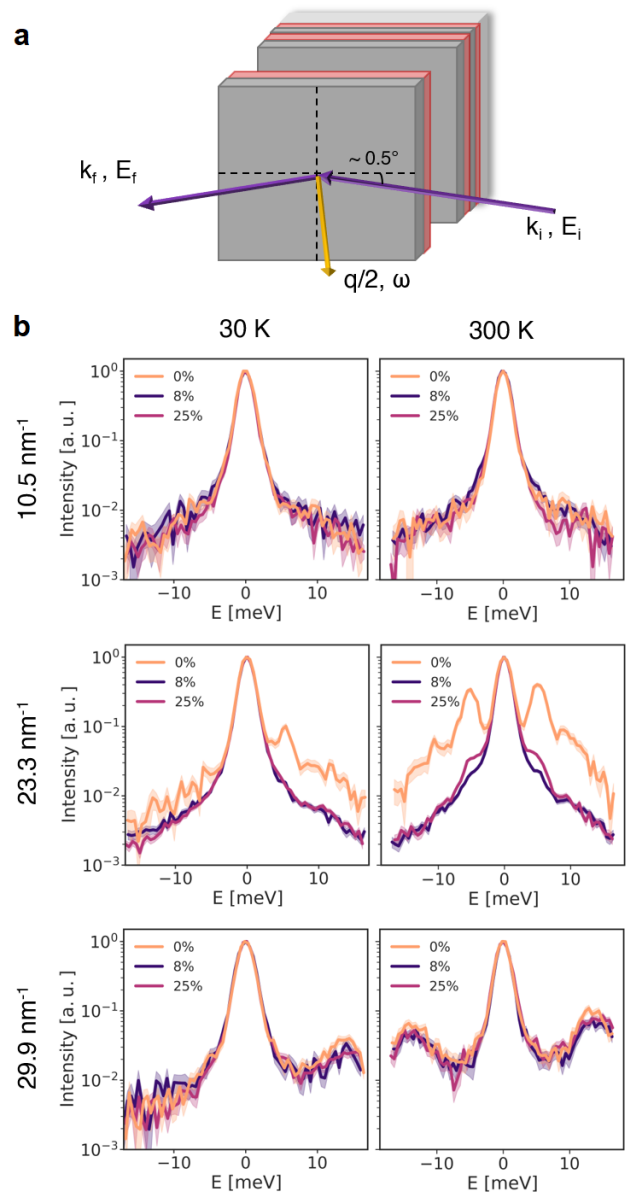


Figure 2. **GI-IXS of the GaAs/AlAs SLs.** **a**, Scattering geometry of the synchrotron-based GI-IXS on the SLs. **b**, Comparison of constant- q scans of samples with 0%, 8% and 25% ErAs nanodot density at representative q values at 30 K (left column) and 300 K (right column). At medium- q regime near $q = 23.3 \text{ nm}^{-1}$, there is a noticeable departure of the phonon spectra between the disordered SLs and the Ref-SL. Most importantly, the intensity ratio between the Stokes and the anti-Stokes peaks show anomalous behavior in disordered samples at low temperature. The intensity is normalized and shaded pale regions indicate one standard deviation.

conclusions so far can be drawn from raw data prior to further data analysis.

Observation of localization-thermalization crossover. To reinforce the aforementioned claims, we quantify the

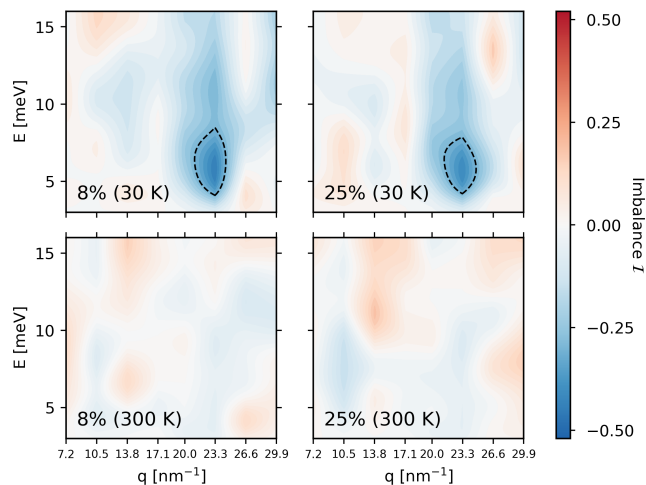


Figure 3. **Phonon population imbalance in energy and wavevector parameter space.** Phonon population imbalance \mathcal{I} for ErAs-disordered SLs (8%, left column, and 25%, right column) as defined in Eq. (1). The imbalance is extracted using the data in Fig. 2. The high imbalance \mathcal{I} is only observed at low temperature (top row) but not at room temperature (bottom row), while the two disordered SLs show large imbalance up to $|\mathcal{I}| \sim 0.5$ in similar energy window near $E = 6$ meV and wavevector window $q = 23 \text{ nm}^{-1}$. The dashed lines denote the contour for $|\mathcal{I}| = 0.3$.

difference in behavior of the Stokes and the anti-Stokes peak intensities between the Ref and disordered samples. The ratio $R = I(\text{Stokes})/I(\text{anti-Stokes})$ for each sample is determined from the GI-IXS spectra as a function of the phonon energy for each constant- q scan. The calculation of R is performed without removing the elastic peak to preclude any undesirable artifacts that could arise from elastic-peak subtraction. The phonons in the Ref SL follow equilibrium statistics based on previous evidence [37]. The data are presented to display energy ranges outside those which may be significantly impinged by the elastic peak. To characterize the phonon population imbalance of the disordered samples, we define an imbalance parameter, similar to other studies [53, 54], as

$$\mathcal{I} = \frac{R_{\text{Disorder}} - R_{\text{Ref}}}{R_{\text{Disorder}} + R_{\text{Ref}}}, \quad (1)$$

where R_{Ref} refers to the Ref SL and R_{Disorder} refers to disordered SLs with either 8% or 25% disorder density by area coverage. Plots of this parameter in energy-wavevector space for both disordered samples are shown in Fig. 3. Both display $|\mathcal{I}| < 0.15$ at all measured energies and wavevectors at room temperature, where localization is not expected due to strong temperature effects towards equilibrium.

As noted from the GI-IXS spectra, the largest imbalance in the phonon population occurs near $q = 23.3 \text{ nm}^{-1}$, reaching absolute values up to $|\mathcal{I}| \sim 0.5$. This value is comparable to analogous number imbalance

measurements within the MBL phase in ultracold atom experiments [10, 11]. The SL with lower disorder density (8%) appears to experience slightly larger imbalance in a more prominent region in energy-wavevector phase space, but the general trend between the two disordered samples is very similar. Moreover, in addition to the population imbalance taking place within a medium- q window, the behavior also occurs in a finite energy interval between ~ 4 -13 meV. Fig. 3 shows distinct regimes in the energy-wavevector phase space with large (dark blue) or weak (light colors) imbalance, which may further serve as a boundary between MBL and thermal phases. As the phononic SL system on a substrate is more akin to an open quantum system, one expects a crossover behavior instead of a sharp transition between the thermal and the MBL phases as in a closed quantum system. Nevertheless, the suppression of phonon population at medium- q regime is indicative of a possible reduction in the effective dimensionality of the site-Hilbert space, which could be a manifestation of a strong local repulsion (Fig. 2b).

Effective phonon action in disordered SLs. To gain further insight on the phonon behavior, we develop a minimal model for the phonon transport in the disordered quasi-1D SL system using a tight-binding description. The suitability of the tight-binding approach can be justified as the computed minimum localization length of ~ 20 nm in disordered SL samples [41] is comparable to the characteristic length scale of the SL system with a superperiodicity of 6 nm. The tight-binding phonon Hamiltonian of the Ref SL can be written as

$$H_0 = \sum_i \varepsilon_i n_i + \sum_i t_i \left(a_{i+1}^\dagger a_i + a_i^\dagger a_{i+1} \right), \quad (2)$$

where ε_i is the on-site energy of the i^{th} SL layer, $n_i = a_i^\dagger a_i$ is the local phonon population, and t_i is the hopping amplitude between the neighboring SL layers. We further introduce the disorder-field Hamiltonian H_d and the phonon-disorder interaction Hamiltonian H_I as

$$\begin{aligned} H_d &= \frac{1}{2} \sum_i \varepsilon_{d,i} \xi_i^2 \\ H_I &= \sum_i g_i a_i^\dagger a_i \xi_i, \end{aligned} \quad (3)$$

where $\varepsilon_{d,i} > 0$ is the on-site disorder energy of the i^{th} SL layer, ξ_i is the disorder field, and g_i is the local phonon-disorder coupling strength. The on-site disorder energy $\varepsilon_{d,i}$ is appropriate due to the mass difference by the ErAs nanodots. The phonon-disorder coupling is proportional to the phonon population n_i , which is also reasonable.

For comprehensive impurity average calculation, either replica theory [55, 56], or Keldysh formalism [57], or supersymmetry method [58] shall be implemented. Here for a qualitative estimate without loss of generality, we

define the effective phonon action S_{eff} by integrating over the disorder degrees of freedom:

$$e^{-S_{\text{eff}}} = e^{-S_0} \times \int D\xi e^{-S_d[\xi] - S_I[\xi]}, \quad (4)$$

where $D\xi = \prod_i d\xi_i$ is the functional measure of the disorder configurations. Such simpler treatment makes the disorder field resemble annealed disorder with internal excitation energies. By carrying out an explicit calculation of Eq. (4), we obtain the following effective phonon Hamiltonian

$$H = \sum_i \left(\varepsilon_i + \frac{g_i^2}{2\varepsilon_{d,i}} \right) n_i + \sum_i t_i \left(a_{i+1}^\dagger a_i + a_i^\dagger a_{i+1} \right) + \frac{1}{2} \sum_i \frac{g_i^2}{\varepsilon_{d,i}} (n_i^2 - n_i). \quad (5)$$

where we assumed a zero temperature to simplify the Matsubara frequency calculations. By defining

$$\begin{aligned} J &= -t_i \\ U_i &= \frac{g_i^2}{\varepsilon_{d,i}} \\ \mu_i &= \varepsilon_i + \frac{g_i^2}{2\varepsilon_{d,i}}, \end{aligned} \quad (6)$$

we see that Eq. (5) can be exactly rewritten in terms of the standard 1D Bose-Hubbard model

$$H_{\text{Bose-Hubbard}} = \sum_i \mu_i n_i - J \sum_i \left(a_{i+1}^\dagger a_i + a_i^\dagger a_{i+1} \right) + \frac{1}{2} \sum_i U_i (n_i^2 - n_i), \quad (7)$$

but with a disordered on-site chemical potential μ_i and on-site interaction strength U_i . This model has been extensively studied and shown to exhibit an MBL phase [59, 60]. Furthermore, the MBL in this model is characterized by an *inverted* mobility edge in which higher energy states are localized [61, 62], similar to what is observed in our GI-IXS experiment.

The on-site repulsion U_i in Eq. (7) is an important parameter controlling the model behavior, and can be estimated as (Supplemental Material [63])

$$U_i \propto \frac{R^2}{N n_B(\varepsilon_{d,i})} \sqrt{\frac{m_{\text{Er}}}{m_{\text{eff}}}}, \quad (8)$$

where R is the nanodot radius, n_B is the Bose-Einstein distribution, m_{Er} is the mass of Er atom from disorders and m_{eff} is the effective mass from Al and Ga atoms from Ref SLs, and N denotes the system size. A number of experimental features can be reconciled with Eq. (8). First, the disorder concentration η is cancelled out and absent in Eq. (8), which is consistent with the similar behavior observed in our 8% and 25% samples

in the parameter regime with large phonon population imbalance. Second, the large mass differences between Er atoms and the Ga and Al atoms tends to increase U_i and favors MBL. Third, the large disorder radius R with an R^2 -dependence also facilitates a large U_i . Lastly, a lower phonon population inside the disorder $n_B(\varepsilon_{d,i})$ can generate a larger U_i , which agrees with the observation that at medium- q phonon population is suppressed while imbalance \mathcal{I} is high. The possibility to exactly map the strongly disordered quasi-1D phonon transport into the Bose-Hubbard model, as well as the guideline to increase on-site repulsion using Eq. (8), hints at a new avenue to seek MBL in disordered SL solid-state systems.

Discussion. In our SL system, the natural choice of system size is the total period of SL $N = 300$. However, coherent phonon behavior can be observed in an $N = 16$ SL [37], within which the inter-SL transport can be "coarse-grained" as one effective site. In accordance with the long phonon coherence and long phonon mean-free-path l_{MFP} in an SL with total thickness L [38], the effective system size for a $N = 300$ period SL gives $N_{\text{eff}} = N l_{\text{MFP}} / L < 20$, which serves the role of N in Eq. (8) and further increases the on-site repulsion. In addition, the observed imbalance \mathcal{I} takes on an extreme value near $E = 5$ meV, with $\mathcal{I} = -0.5$, while it diminishes to $\mathcal{I} = -0.15$ near $E = 15$ meV, indicating the existence of two mobility edges in energy. Although the 1D Bose-Hubbard model only has one inverted mobility edge, the additional mobility edge can be intuitively understood as resulting from high-energy extended modes which can be added to Eq. (2) as longer-range hopping terms. This behavior qualitatively agrees with the self-consistent diagrammatic theory of phonon localization in hard-sphere scatterers [29], and semi-quantitatively with the non-equilibrium Green's function calculations in this SL system showing the localization regime at around 6 to 10 meV [38]. On the other hand, the localization window in wavevector space has not been predicted since theories either integrate over momentum degrees of freedom or set the momentum to zero for simplicity [28, 29]. In our 6 nm superperiodic SL, $q \sim 20 \text{ nm}^{-1}$ corresponds to a ~ 40 -fold extended Brillouin zone. From the computed SL phonon dispersion [41], this enters into the phonon energy at $E \sim 10$ meV, above the lower-energy delocalized regime. Consequently, the localization window in wavevector space may naturally be linked to the localization window in energy space.

Conclusion. In summary, we provide mode-resolved evidence of signatures of many-body localization in disordered semiconducting phononic SLs, through state-of-the-art low temperature GI-IXS measurements. The disordered SL platform contains the essential elements that can lead to the realization of MBL: a reduced dimen-

sionality which limits the pathways to drive the system towards thermal equilibrium, while the nanodot-type disorder with size comparable to the SL spacing can provide strong on-site interaction and strong disorder effects. By investigating the quasiparticle population imbalance, we uncover that phonons in the disordered SL samples fail to thermalize within finite energy and wavevector windows. This likening of the experimental observations to the MBL phenomenology is further supported by theoretical calculations showing the equivalence between the quasi-1D tight-binding phonon transport under strong disorder and the 1D Bose-Hubbard model with a known MBL phase. In particular, our experimental findings qualitatively agree with the criteria to reach high on-site repulsion that favors an MBL phase. Our study opens up new opportunities in two directions: as a new experimental solid-state platform for realizing possible MBL phenomena, and as a novel phonon phase far away from equilibrium.

ACKNOWLEDGMENTS

The authors thank R. Nandkishore and P. Cappellaro for helpful discussions. T.N., N.A., N.C.D. and M.L. acknowledge the support from U.S. DOE, Office of Science (SC), Basic Energy Sciences (BES), award No. DE-SC0020148. N.A. acknowledges the support of the National Science Foundation Graduate Research Fellowship Program under Grant No. 1122374. H.C.P. is supported by a Pappalardo Fellowship at MIT and a Croucher Foundation Fellowship. Work of Y.T. was supported by Solid State Solar-Thermal Energy Conversion Center (S3TEC), an Energy Frontier Research Center funded by the U.S. Department of Energy, Office of Science, Office of Basic Energy Sciences under Award DE-SC0001299 (prior to January 2019). A.C., Y.Q.C., L.W., J.G., and Y. Z. acknowledge the support from DOE/BES, the Materials Science and Engineering Divisions, under Contract No. DE-SC0012704. This research used resources of the Advanced Photon Source, a U.S. DOE Office of Science User Facility operated for the DOE Office of Science by Argonne National Laboratory under Contract No. DE-AC02-06CH11357.

* Corresponding authors.
mingda@mit.edu, sjh5899@psu.edu

- [1] D. M. Basko, I. L. Aleiner, and B. L. Altshuler, *Ann. Phys.* **321**, 1126 (2006).
- [2] A. Pal and D. A. Huse, *Phys. Rev. B* **82**, 174411 (2010).
- [3] R. Nandkishore and D. A. Huse, *Annu. Rev. Condens. Matter Phys.* **6**, 15 (2015).
- [4] D. A. Abanin, E. Altman, I. Bloch, and M. Serbyn, *Rev. Mod. Phys.* **91**, 021001 (2019).
- [5] V. Khemani, M. Hermele, and R. Nandkishore, *Phys. Rev. B* **101**, 174204 (2020).
- [6] D. A. Huse, R. Nandkishore, V. Oganesyan, A. Pal, and S. L. Sondhi, *Phys. Rev. B* **88**, 014206 (2013).
- [7] A. Chandran, V. Khemani, C. R. Laumann, and S. L. Sondhi, *Phys. Rev. B* **89**, 144201 (2014).
- [8] D. Pekker, G. Refael, E. Altman, E. Demler, and V. Oganesyan, *Phys. Rev. X* **4**, 011052 (2014).
- [9] S. Kondov, W. McGehee, W. Xu, and B. DeMarco, *Phys. Rev. Lett.* **114**, 083002 (2015).
- [10] M. Schreiber, S. S. Hodgman, P. Bordia, H. P. Lüschen, M. H. Fischer, R. Vosk, E. Altman, U. Schneider, and I. Bloch, *Science* **349**, 842 (2015).
- [11] J. Y. Choi, S. Hild, J. Zeiher, P. Schauß, A. Rubio-Abadal, T. Yefsah, V. Khemani, D. A. Huse, I. Bloch, and C. Gross, *Science* **352**, 1547 (2016).
- [12] A. Lukin, M. Rispoli, R. Schittko, M. E. Tai, A. M. Kaufman, S. Choi, V. Khemani, J. Léonard, and M. Greiner, *Science* **364**, 256 (2019).
- [13] M. Rispoli, A. Lukin, R. Schittko, S. Kim, M. E. Tai, J. Léonard, and M. Greiner, *Nature* **573**, 385 (2019).
- [14] J. Smith, A. Lee, P. Richerme, B. Neyenhuis, P. W. Hess, P. Hauke, M. Heyl, D. A. Huse, and C. Monroe, *Nat. Phys.* **12**, 907 (2016).
- [15] K. X. Wei, C. Ramanathan, and P. Cappellaro, *Phys. Rev. Lett.* **120**, 070501 (2018).
- [16] P. Roushan, C. Neill, J. Tangpanitanon, V. M. Bastidas, A. Megrant, R. Barends, Y. Chen, Z. Chen, B. Chiaro, A. Dunsworth, A. Fowler, B. Foxen, M. Giustina, E. Jeffrey, J. Kelly, E. Lucero, J. Mutus, M. Neeley, C. Quintana, D. Sank, A. Vainsencher, J. Wenner, T. White, H. Neven, D. G. Angelakis, and J. Martinis, *Science* **358**, 1175 (2017).
- [17] K. Xu, J.-J. Chen, Y. Zeng, Y.-R. Zhang, C. Song, W. Liu, Q. Guo, P. Zhang, D. Xu, H. Deng, K. Huang, H. Wang, X. Zhu, D. Zheng, and H. Fan, *Phys. Rev. Lett.* **120**, 050507 (2018).
- [18] R. Nandkishore and S. Gopalakrishnan, *Ann. Phys.* **529**, 1600181 (2017).
- [19] P. W. Anderson, *Phys. Rev.* **109**, 1492 (1958).
- [20] E. Abrahams, P. W. Anderson, D. C. Licciardello, and T. V. Ramakrishnan, *Phys. Rev. Lett.* **42**, 673 (1979).
- [21] P. A. Lee and T. V. Ramakrishnan, *Rev. Mod. Phys.* **57**, 287 (1985).
- [22] M. Cutler and N. F. Mott, *Physical Review* **181**, 1336 (1969).
- [23] D. J. Thouless, *Phys. Rep.* **13**, 93 (1974).
- [24] B. Sutherland, *Phys. Rev. B* **34**, 5208 (1986).
- [25] S. John, *Phys. Rev. Lett.* **58**, 2486 (1987).
- [26] R. L. Weaver, *Wave Motion* **12**, 129 (1990).
- [27] L. Sanchez-Palencia, D. Clément, P. Lugan, P. Bouyer, G. V. Shlyapnikov, and A. Aspect, *Phys. Rev. Lett.* **98**, 210401 (2007).
- [28] S. John, H. Sompolinsky, and M. J. Stephen, *Phys. Rev. B* **27**, 5592 (1983).
- [29] T. R. Kirkpatrick, *Phys. Rev. B* **31**, 5746 (1985).
- [30] P. Sheng, M. Zhou, and Z.-Q. Zhang, *Phys. Rev. Lett.* **72**, 234 (1994).
- [31] M. P. V. Albada and A. Lagendijk, *Phys. Rev. Lett.* **55**, 2692 (1985).
- [32] P.-E. Wolf and G. Maret, *Phys. Rev. Lett.* **55**, 2696 (1985).

- [33] D. S. Wiersma, P. Bartolini, A. Lagendijk, and R. Righini, *Nature* **390**, 671 (1997).
- [34] T. Schwartz, G. Bartal, S. Fishman, and M. Segev, *Nature* **446**, 52 (2007).
- [35] M. Segev, Y. Silberberg, and D. N. Christodoulides, *Nat. Photonics* **7**, 197 (2013).
- [36] H. Hu, A. Strybulevych, J. H. Page, S. E. Skipetrov, and B. A. van Tiggelen, *Nat. Phys.* **4**, 945 (2008).
- [37] M. N. Luckyanova, J. Garg, K. Esfarjani, A. Jandl, M. T. Bulsara, A. J. Schmidt, A. J. Minnich, S. Chen, M. S. Dresselhaus, Z. Ren, E. A. Fitzgerald, and G. Chen, *Science* **338**, 936 (2012).
- [38] J. Mendoza and G. Chen, *Nano Lett.* **16**, 7616 (2016).
- [39] S. Hu, Z. Zhang, P. Jiang, J. Chen, S. Volz, M. Nomura, and B. Li, *J. Phys. Chem. Lett.* **9**, 3959 (2018).
- [40] T. Juntunen, O. Vänskä, and I. Tittonen, *Phys. Rev. Lett.* **122**, 105901 (2019).
- [41] M. N. Luckyanova, J. Mendoza, H. Lu, B. Song, S. Huang, J. Zhou, M. Li, Y. Dong, H. Zhou, J. Gallow, L. Wu, B. J. Kirby, A. J. Grutter, A. A. Puretzky, Y. Zhu, M. S. Dresselhaus, A. Gossard, and G. Chen, *Sci. Adv.* **4**, eaat9460 (2018).
- [42] M. Maldovan, *Nature* **503**, 209 (2013).
- [43] J. Serrano, A. Bosak, M. Krisch, F. J. Manjón, A. H. Romero, N. Garro, X. Wang, A. Yoshikawa, and M. Kuball, *Phys. Rev. Lett.* **106**, 205501 (2011).
- [44] D. Rossini, A. Silva, G. Mussardo, and G. E. Santoro, *Phys. Rev. Lett.* **102**, 127204 (2009).
- [45] E. Canovi, D. Rossini, R. Fazio, G. E. Santoro, and A. Silva, *New J. Phys.* **14**, 095020 (2012).
- [46] Z. Lenarčič, O. Alberton, A. Rosch, and E. Altman, [arXiv:1910.01548 \[cond-mat\]](https://arxiv.org/abs/1910.01548) (2019).
- [47] H. Sinn, E. Alp, A. Alatas, J. Barraza, G. Bortel, E. Burkel, D. Shu, W. Sturhahn, J. Sutter, T. Toellner, and J. Zhao, *Nuc. Instrum. Meth. A* **467-468**, 1545 (2001).
- [48] A. Alatas, B. Leu, J. Zhao, H. Yavas, T. Toellner, and E. Alp, *Nuc. Instrum. Meth. A* **649**, 166 (2011).
- [49] T. S. Toellner, A. Alatas, and A. H. Said, *J. Synchrotron Radiat.* **18**, 605 (2011).
- [50] H. Sinn, *J. Phys. Condens. Matter* **13**, 7525 (2001).
- [51] T. Goldstein, S.-Y. Chen, J. Tong, D. Xiao, A. Ramasubramaniam, and J. Yan, *Scientific Reports* **6**, 1 (2016).
- [52] A. De Francesco, L. Scaccia, M. Maccarini, F. Formisano, Y. Zhang, O. Gang, D. Nykypanchuk, A. H. Said, B. M. Leu, A. Alatas, Y. Q. Cai, and A. Cunsolo, *ACS Nano* **12**, 8867 (2018).
- [53] E. Levi, M. Heyl, I. Lesanovsky, and J. P. Garrahan, *Phys. Rev. Lett.* **116**, 237203 (2016).
- [54] H. P. Lüschen, P. Bordia, S. S. Hodgman, M. Schreiber, S. Sarkar, A. J. Daley, M. H. Fischer, E. Altman, I. Bloch, and U. Schneider, *Phys. Rev. X* **7**, 011034 (2017).
- [55] M. Mezard, G. Parisi, and M. A. Virasoro, *Spin Glass Theory and Beyond: An Introduction To The Replica Method and Its Applications* (World Scientific, New Jersey, 1987).
- [56] V. Dotsenko, *Introduction to the Replica Theory of Disordered Statistical Systems* (Cambridge University Press, New York, 2001).
- [57] A. Kamenev, *Field Theory of Non-Equilibrium Systems* (Cambridge University Press, 2011).
- [58] K. Efetov, *Adv. Phys.* **32**, 53 (1983).
- [59] V. Michal, B. Altshuler, and G. Shlyapnikov, *Phys. Rev. Lett.* **113**, 045304 (2014).
- [60] V. P. Michal, I. L. Aleiner, B. L. Altshuler, and G. V. Shlyapnikov, *Proc. Natl. Acad. Sci. U.S.A.* **113**, E4455 (2016).
- [61] P. Sierant, D. Delande, and J. Zakrzewski, *Phys. Rev. A* **95**, 021601 (2017).
- [62] P. Sierant and J. Zakrzewski, *New J. Phys.* **20**, 043032 (2018).
- [63] See Supplementary Material for further details on the estimate of the on-site repulsion, which includes Ref. [64].
- [64] S. V. Fal'eev and F. Léonard, *Physical Review B* **77**, 214304 (2008).

**SUPPLEMENTAL MATERIALS FOR SIGNATURE OF MANY-BODY LOCALIZATION OF PHONONS
IN STRONGLY DISORDERED SUPERLATTICES**

Parameter estimation of the strong Hubbard interaction

To evaluate the magnitudes of the parameters, particularly the origin of strong on-site repulsion U_i , we carry out a simple estimation as follows. For the phonon-disorder interaction Hamiltonian H_I , the first-order self-energy for the i^{th} SL layer can be computed as

$$\Sigma_i^1(\omega) = g_i^2 \left[\frac{n_B(\varepsilon_{d,i}) + n_B(\varepsilon_i)}{\omega - \varepsilon_i + \varepsilon_{d,i}} + \frac{n_B(\varepsilon_{d,i}) - n_B(\varepsilon_i) + 1}{\omega - \varepsilon_i - \varepsilon_{d,i}} \right] \quad (\text{S1})$$

where n_B is the Bose-Einstein distribution function. If we assume that the energy of disorder at a given SL layer is much smaller than the energy of SL, $\varepsilon_{d,i} \ll \varepsilon_i$, Eq. (S1) can be greatly simplified as

$$\Sigma_i^1(\omega) \sim 2g_i^2 \frac{n_B(\varepsilon_{d,i})}{\omega - \varepsilon_i} \quad (\text{S2})$$

The corresponding relaxation time can be computed as the imaginary part of Eq. (S2). The relaxation time of the i^{th} SL layer τ_i can be written as

$$\frac{1}{\tau_i} = 4\pi g_i^2 n_B(\varepsilon_{d,i}) \nu(\varepsilon_i) \quad (\text{S3})$$

where $\nu(\varepsilon_i)$ is the density-of-state in the i^{th} SL. Further assuming a Matthiessen's rule that the total relaxation rate $\frac{1}{\tau}$ is the sum for each layer, we have $1/\tau \sim N/\tau_i$ if assuming other quantities are layer-independent or drawn from an independent random distribution. On the other hand, for phonon scattering with finite-sized nanodot disorders, in the regime $qR > 1$, where q is the phonon wavevector and R is the disorder radius, it is known that the geometrical scattering will dominate [64], such that

$$\frac{1}{\tau_0} = 2\pi\eta v_s R^2 \quad (\text{S4})$$

in which v_s is the sound velocity. Since Eq. (S4) and Eq. (S3) are derived differently but represent the same context for disorder scattering, we can assume that $1/\tau \propto 1/\tau_0$ without loss of generality. As a result, we have

$$g_i^2 \propto \frac{\eta v_s R^2}{2N n_B(\varepsilon_{d,i}) \nu(\varepsilon_i)} \quad (\text{S5})$$

For the non-interacting disorder part H_d , we adopt a total energy argument: the added disorder creates the energy that is proportional to the disorder concentration η , while the phonon energy is inversely proportional to the square root of the mass, $\varepsilon \propto \sqrt{\frac{1}{m}}$. As a result, the total disorder energy $\varepsilon_{d,i}$ and the SL phonon energy ε_i are linked as

$$\varepsilon_{d,i} \propto \eta \sqrt{\frac{m_{\text{eff}}}{m_{\text{Er}}}} \varepsilon_i \quad (\text{S6})$$

where if we focus on phonon modes of Er, Ga and Al atoms, $m_{\text{eff}} = m_{\text{Ga}} m_{\text{Al}} / (m_{\text{Ga}} + m_{\text{Al}})$ is the effective mass of SL.

Finally, using Eqs. (S6) and (S5), we have the on-site repulsion

$$U_i = \frac{g_i^2}{\varepsilon_{d,i}} \propto \frac{\nu_s R^2}{N n_B(\varepsilon_{d,i}) \nu(\varepsilon_i) \varepsilon_i} \sqrt{\frac{m_{\text{Er}}}{m_{\text{eff}}}} \quad (\text{S7})$$

From Eq. (S7), we can see a number of notable features that are directly associated with experimental observations, discussed in main text.

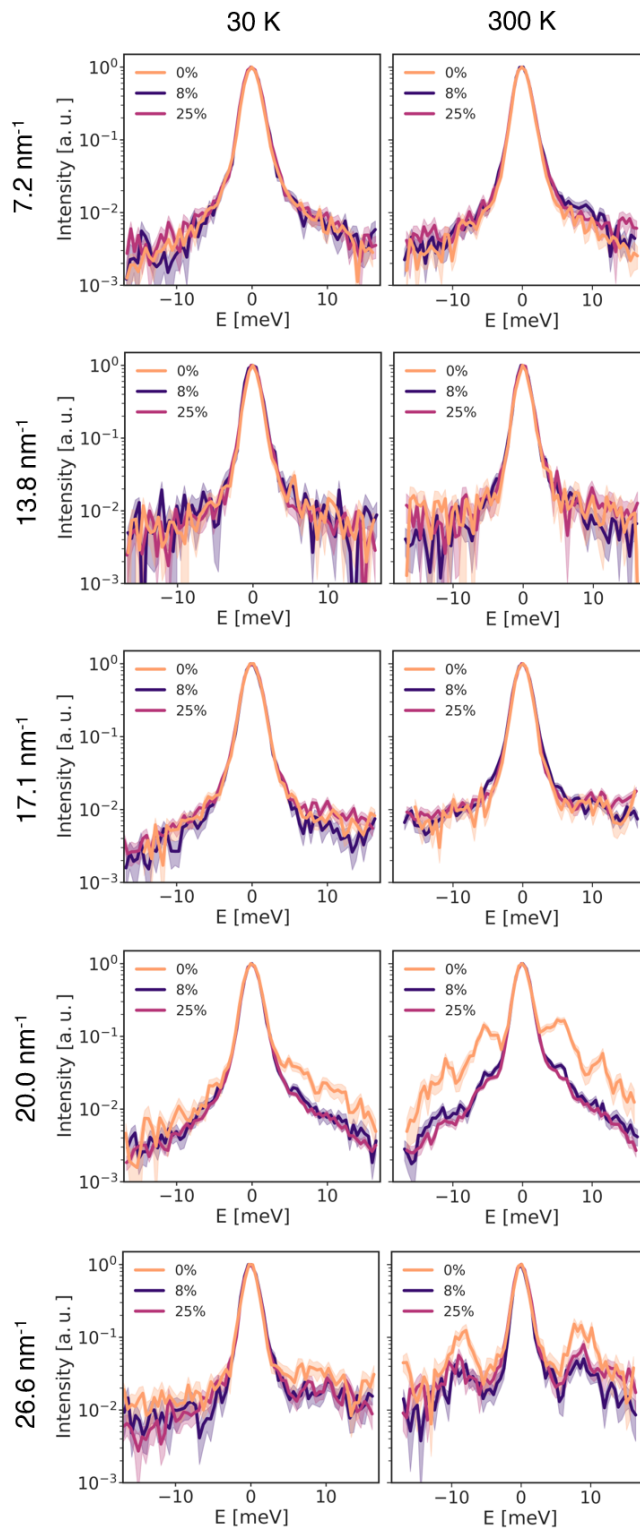


Figure S1. GI-IXS scans at constant- q for samples with 0%, 8% and 25% ErAs at 30 K and 300K. The intensity is normalized and the pale regions indicate one standard deviation.

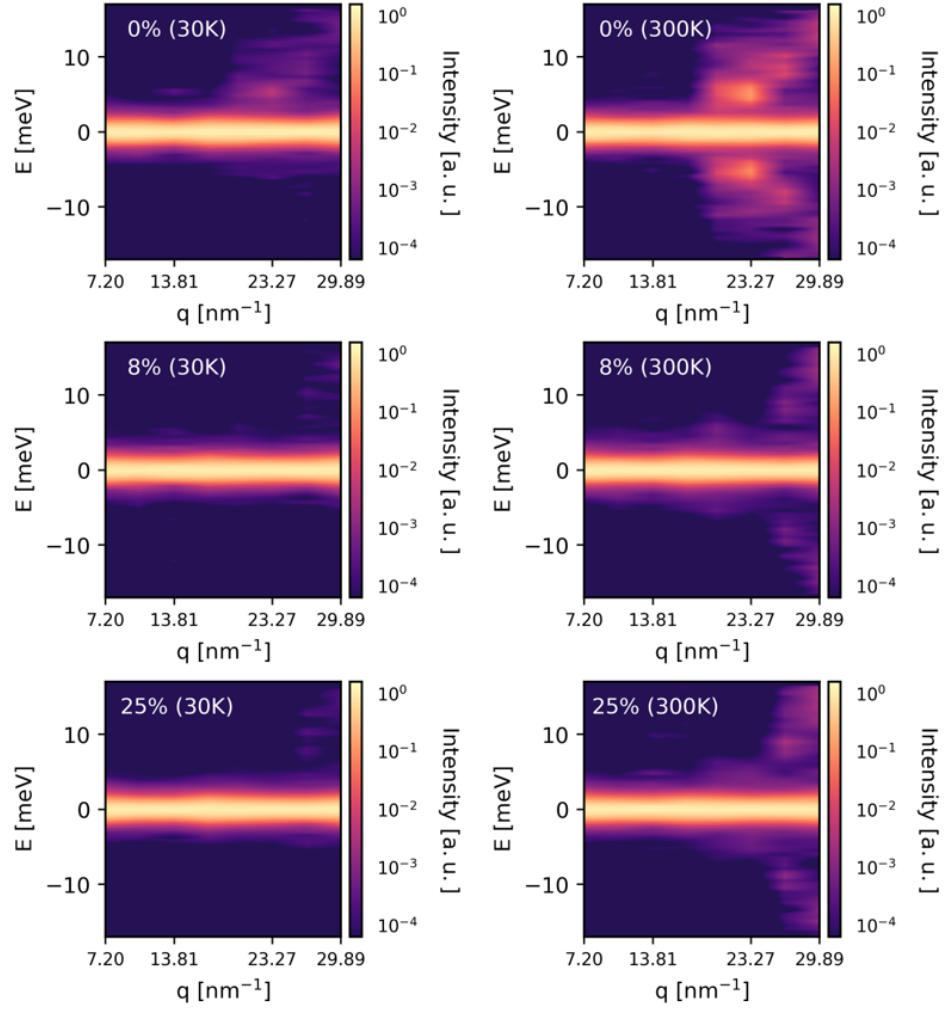


Figure S2. Phonon dispersion relations obtained from GI-IXS spectra at 30 K and 300 K for samples with 0%, 8% and 25% ErAs. The colormap is representative of the normalized intensity in log-scale.